Compact finite difference modeling of 2-D acoustic wave propagation

L. J. Córdova[a], O. Rojas[b], B. Otero[c], J. Castillo[d]

[a] *Universidad de Oriente, Dpto. de Matemática, Cumaná, Sucre, Venezuela*
[b] *Universidad Central de Venezuela, Facultad de Ciencias, Escuela de Computación, Caracas, Venezuela*
[c] *Universitat Politecnica of Catalonia, Campus Nord, Dpto. de Arquitectura de Computadores, Barcelona, Spain*
[d] *San Diego State University, 5500 Campanile Drive, San Diego CA, 92182-7720*

Abstract

We present two fourth-order compact finite difference (CFD) discretizations of the velocity-pressure formulation of the acoustic wave equation in 2-D rectangular grids. The first method uses standard implicit CFD on nodal meshes and requires solving tridiagonal linear systems along each grid line, while the second scheme employs a novel set of mimetic CFD operators for explicit differentiation on staggered grids. Both schemes share a Crank-Nicolson time integration decoupled by the Peaceman-Rachford splitting technique to update discrete fields by alternating the coordinate direction of CFD differentiation (ADI-like iterations). For comparison purposes, we also implement a spatially fourth-order FD scheme using non compact staggered mimetic operators in combination to second-order Leap-frog time discretization. We apply these three schemes to model acoustic motion under homogeneous boundary conditions and compare their experimental convergence and execution times, as grid is successively refined. Both CFD schemes show four-order convergence, with a slight superiority of the mimetic version, that leads to more accurate results on fine grids. Conversely, the mimetic Leap-frog method only achieves quadratic convergence and shows similar accuracy to CFD results exclusively on coarse grids. We finally observe that computation times of nodal CFD simulations are between four and five times higher than those spent by the mimetic CFD scheme with similar grid size. This significant performance difference is attributed to solving those embedded linear systems inherent to implicit CFD.

Keywords: Compact schemes, mimetic finite differences, acoustic media, ADI methods.

1. Introduction

Wave motion in an acoustic medium with density ρ and adiabatic compression modulus k can be modeled by the system

$$\begin{cases} \frac{1}{k}\frac{\partial u}{\partial t} = -\nabla \cdot \vec{v} + f, \\ \rho \frac{\partial \vec{v}}{\partial t} = -\nabla u \end{cases} \tag{1}$$

Email addresses: lcordova14@gmail.com (L. J. Córdova), rojasotilio@gmail.com (O. Rojas), botero@ac.upc.edu (B. Otero), castillo@myth.sdsu.edu (J. Castillo)

where dependent variables correspond to the particle velocity vector $\vec{v} = (v, w)$ and the pressure field u. This velocity-pressure formulation allows stating any consistent combination of free-surface or rigid-wall boundary conditions on the appropriate physical variable. Current finite difference (FD) methods for this model are mostly implemented on spatial staggered grids, and use explicit time discretization performed by short second-order stencils, in order to limit memory computer requirements. Applications covers from seismic imaging of Earth interior [6] [12], visualization of sound fields [29], and seismic motion in marine scenarios [31] [35]. In a staggered grid, wave fields and material parameters are defined at intermediate grid positions, in such a way that an unknown field is located at the center of those it depends. Numerical differentiation exploits this geometrical distribution that halves the grid spacing to gain accuracy. FD staggered-grid modeling of wave propagation on heterogeneous media having drastic variation of material properties has exhibits minimal dispersion and numerical anisotropy in the more general case of elastic rheologies [33]. These numerical techniques can achieve further accuracy by employing large computational stencils with fourth or even higher order. Now, this practice might require of more time-consuming domain decomposition procedures in parallel FD applications, because of the higher demand of data interchange. In addition, high order FD discretization of Neumann boundary conditions based on lateral stencils can degenerate in numerical instabilities on wave propagation problems [13] [14] [26].

As an alternative, implicit compact FD methods can accomplish high-order accuracy by solving for the spatial derivatives, a linear system along each gridline. In a compact FD approximation, the discrete differential values at subsequent grid points are coupled, and the difference formula requires fewer grid points than those used by explicit FD stencils. A general family of compact schemes have attained fast implementations after including the alternating direction implicit (ADI) methodology. ADI methods were introduced by Peaceman, Rachford, and Douglas [10] [22] for 2-D diffusion problems in infinite domains, and their formulation is unconditionally stable and well suited for efficient implementations. These pioneer works have been followed by emerging formulations of higher order compact-ADI FD with moderate computational cost, and some recent contributions are [9] [16] [17] [24]. At the implementation level, the main drawback of these strategies is the simultaneous approximation of derivate values at all points along a grid line by solving a linear (usually tridiagonal) system. Although, this problem can be solved cheaply and precisely by efficient methods based on Thomas' algorithm. As an effort to develop conservative FD, Castillo and collaborators have proposed the mimetic differentiation formulas on staggered grids that provide second-, fourth-, and sixth-order accuracy at all grid locations including boundaries [3] [4]. Among several applications of mimetic FD, fourth-order modeling of surface waves and earthquake ruptures on elastic media count as related to methods presented in this paper [25] [26]. Recently, Abouali and Castillo introduce a compact factorization of the high-order mimetic operators in terms of the second-order ones and additional auxiliary operators [1]. Both latter operators exhibit shorter stencils compared to the provided by the formers, and represent compact choices for explicit differentiation.

In this paper, we implement and compare three numerical methods to solve the velocity-pressure acoustic system on rectangular domains. All of them present fourth-order spatial differentiation. The first method uses implicit compact FD on nodal grids similar to those proposed by [7] [20], in combination to a Crank-Nicolson time integration

efficiently solved by a Peaceman-Rachford ADI decomposition. The second method shares same time-stepping strategy, but applies explicit compact mimetic FD to reduce computer execution times. This scheme represents the first 2-D application of such differentation operators. Both compact formulations are detailed in section 2 of this paper. Section 3 briefly describes our last scheme based on non-compact mimetic differentiation coupled to a second-order Leap-frog discretization of time derivatives. This third numerical method falls into the family of modern space-time staggered FD methods on wave propagation, and its results as used as a reference. Section 4 presents numerical solutions to a test case with homogeneous Dirichlet boundary conditions, and compares accuracy and convergence achieved by these three methods. Finally, section 5 summarizes our conclusions and point out some extensions of this work.

2. Formulation of compact finite difference (CFD) methods

In this section, we revise standard fourth-order operators for compact finite differentiation of a smooth field given discretely on a 1-D nodal grid, and use them to formulate a numerical scheme for the 2-D acoustic model stated by Eqs. (2) and (3). Next, we present a novel method for this model based on the mimetic compact CFD operators on 1-D staggered grids proposed by Abouali and Castillo in [1] that explicitly carry out the differentiation process without solving any linear system as required by the former implicit CFD on nodal grids. We emphasize this implementation advantage on some final comparative comments on both CFD methods. The benefit of the explicit nature of this new mimetic CFD scheme is later evidenced on reported CPU consumption times in our numerical tests and given in a section below.

2.1. Compact scheme on nodal grids

2.1.1. Review of 1-D operators

Traditional construction mechanisms of CFD are the method of undetermined coefficients applied to Taylor expansions as originally used by Lele in [20], or the combination of local rational approximations (Pade's formulae) as detailed, for instance, in Brio et al. [2]. Instead, we here follow an intuitive formulation of fourth-order CFD operators. Let us consider N equal-sized cells on $[0, 1]$ of width h, and the evaluations u_i of the smooth function $u(x)$ at grid points $x_i = ih$ for $i = 0, ..., N$ and $Nh = 1$. The central FD approximation to $u^{'}(x_i)$ with second order accuracy satisfies

$$u^{'}(x_i) - \frac{u_{i+1} - u_{i-1}}{2h} = \frac{h^2}{6}u^{'''}(x_i) + \frac{h^4}{120}u^4(x_i) + ... \tag{2}$$

Similarly, a Taylor expansion for $u^{'}(x)$ proves that one-third of the difference between $u^{'}(x_i)$ and its average value given by the two nearest neighbours has a second-order leading error term,

$$\frac{1}{3}\left(u^{'}(x_i) - \frac{u^{'}(x_{i+1}) + u^{'}(x_{i-1})}{2}\right) = \frac{h^2}{6}u^{'''}(x_i) - \frac{h^4}{72}u^4(x_i) + ... \tag{3}$$

A direct comparison of eqns. (2) and (3), shows that the following discrete identity holds up to order $O(h^4)$

$$\frac{1}{3}u_{i-1}^{'} + \frac{4}{3}u_{i}^{'} + \frac{1}{3}u_{i+1}^{'} = \frac{u_{i+1} - u_{i-1}}{h} \tag{4}$$

where discrete values $u_i^{'}$ have replaced the evaluations of the exact $u^{'}(x)$. Formula in (4) represents an implicit mechanism of computing simultaneously values $u_i^{'}$ at all grid points if we add some special lateral formulations at boundary closures $i = 0$ and $i = N$. A third-order lateral CFD can be derived by first using the Taylor expansion for $u^{'}(x)$ around x_1 to express the linear combination $2u_0^{'} + 4u_1^{'}$ in the way

$$2u_0^{'} + 4u_1^{'} = 6u_1^{'} - 2hu^{''}(x_1) + h^2u^{'''}(x_1) - \frac{1}{3}h^3u^4(x_1) + ... \tag{5}$$

Then, the term $u_2 - 5u_0$ can be written in a similar manner by means of a new Taylor expansion for $u(x)$ around x_1

$$u_2 - 5u_0 = -4u_1 + 6hu^{'}(x_1) - 2h^2u^{''}(x_1) + h^3u^{'''}(x_1) - \frac{1}{6}h^4u^4(x_1) + ... \tag{6}$$

Equations (5) and (6) easily lead to the following lateral formula

$$2u_0^{'} + 4u_1^{'} = \frac{-5u_0 + 4u_1 + u_2}{h} \tag{7}$$

Coupling the $(N - 1)$ instantiations of (4) at interior nodes to the one-sided approximation in (7) and adding its symmetric version for the right boundary, allow us to compute the whole set of approximate values $u_0^{'}, \ldots, u_N^{'}$ by solving the linear system

$$PU^{'} = QU \tag{8}$$

where vector U collect all given evaluations of $u(x)$ in our lattice, and $U^{'}$ is the resulting vector of nodal approximations to $u^{'}(x)$. Coefficients of compact stencils in (4) and (7) represent the components of $(N + 1)x(N + 1)$ matrices P and Q

$$P = \begin{bmatrix} 2 & 4 & 0 & & \ldots & & 0 \\ 1 & 4 & 1 & 0 & \ldots & & 0 \\ & & & \vdots & & & \\ 0 & & \ldots & 0 & 1 & 4 & 1 \\ 0 & & \ldots & & 0 & 4 & 2 \end{bmatrix}, \quad Q = \frac{1}{h}\begin{bmatrix} -5 & 4 & 1 & 0 & 0 & \ldots & 0 \\ -3 & 0 & 3 & 0 & 0 & \ldots & 0 \\ & & & \vdots & & & \\ 0 & \ldots & 0 & 0 & -3 & 0 & 3 \\ 0 & & \ldots & 0 & 1 & -4 & 5 \end{bmatrix}$$

Above formulation highlights the essence of traditional CFD approximations. A CFD is an implicit formula that relates evaluations of an underlying scalar function to discrete approximations of its derivatives, and it must be solved for the latter values simultaneously on the whole discretization grid. Compared to standard explicit FD, this computational overhead is compensated by the compactness of the difference stencil. For instance, the fourth-order

CFD operator given by eqn. (4) only involves three grid points as opposed to the five-point stencil used on nodal grids for explicit approximation to $u^{'}(x_i)$, and the linear system in (8) is tridiagonal and can be solved by a fast Thomas algorithm. Carpenter and co-workers [7] employed the CFD discretization given by (8) in combination to fourth-order Runge-Kutta (R-K) time integration to solve the 1-D advection equation under an inflow Dirichlet boundary condition. Their results show a global fourth-order convergence in spite of the lower order boundary formulation.

2.1.2. Extension to 2-D with Crank-Nicolson time integration

Nodal CFD discretization of the 2-D acoustic model (1) proceeds on the square grid (x_i, y_j) where $i, j = 0, \cdots, N$ with a common step h along both coordinate axes. Discrete representations of the continuous pressure field u are collected in the matrix $U = [u_{i,j}]$, and similar definitions hold for matrices V and W in the case of the velocity vector (v, w). We denote by U_x and U_y the matrices with approximate components to u_x and u_y, respectively, at all grid nodes. These approximations are computed by using operators P and Q in the matrix calculations

$$U_x P^T \simeq U Q^T, \qquad P U_y \simeq Q U$$

Approximations to u_x are obtained by solving a $(N+1)x(N+1)$ tridiagonal linear system for each row of U_x that includes estimates to u_x at boundary $\partial\Omega$ of $[0,1]\times[0,1]$. In a similar manner is computed each of the $(N+1)$ columns of U_y. Notice that the LU factorization of system matrix P is fundamental for the computational efficiency of this CFD implementation. The availability of estimations of ∇u at $\partial\Omega$ allow the approximation of the velocity vector by the time integration of equation (1) at this boundary. However, $\nabla \cdot \vec{v} = v_x + w_y$ must be approximated only at interior grid nodes because u is given by Dirichlet conditions on $\partial\Omega$. Thus, we need of reduced operators $\bar{P}$ and $\bar{Q}$, where the former is the $(N-1)\times(N-1)$ matrix derived from P after omitting first and last both rows and columns, and the latter is the $(N-1)\times(N+1)$ matrix obtained by neglecting first and last rows of Q. In other words, $\bar{P} = P(1 : N-1, 1 : N-1)$ and results symmetric and positive definite, while $\bar{Q} = Q(1 : N-1, 0 : N)$ inherits a tridiagonal structure from Q. We also consider $\bar{V}$ (with dimensions $(N-1)x(N+1)$) and $\bar{W}$ (with dimensions $(N+1)x(N-1)$) as the reduced versions of approximation matrices V and W, respectively, where we have removed rows (from V) and columns (from W) holding discrete boundary values. CFD approximations to v_x and w_y is achieved by solving $(N-1)$ linear systems to calculate rows of $\bar{V}$, and $(N-1)$ additional linear systems to compute columns of $\bar{W}$

$$\bar{V}_x \bar{P}^T \simeq \bar{V} \bar{Q}^T, \qquad \bar{P} \bar{W}_y \simeq \bar{Q} \bar{W}$$

To formulate the CFD discretization of the acoustic model (1), we introduce the continuous spatial operators

$$A_1 \begin{bmatrix} u \\ v \\ w \end{bmatrix} = \begin{bmatrix} -v_x \\ -u_x \\ 0 \end{bmatrix}, \qquad A_2 \begin{bmatrix} u \\ v \\ w \end{bmatrix} = \begin{bmatrix} -w_y \\ 0 \\ -u_y \end{bmatrix}$$

with corresponding discrete versions

$$A_{1h}\begin{bmatrix}\bar{U}\\V\\W\end{bmatrix} = -\begin{bmatrix}V\bar{Q}^T(\bar{P}^T)^{-1}\\.....\\UQ^T(P^T)^{-1}\\.....\\0\end{bmatrix}, \quad A_{2h}\begin{bmatrix}\bar{U}\\V\\W\end{bmatrix} = -\begin{bmatrix}\bar{P}^{-1}\bar{Q}W\\.....\\0\\.....\\P^{-1}QU\end{bmatrix} \tag{9}$$

No inverse matrix is computed whatsoever in the application of A_{1h} and A_{2h}, and instead matrices on the left hand side are obtained either row-by-row or column-by-column by successively solving linear systems with for either P^T or P, respectively, as mentioned above. We next apply the Crank-Nicolson time discretization and follow the detailed formulation described by Strickwerda in [30] for the 2-D heat equation. This procedure leads to

$$\left(I - \frac{\Delta t}{2}A_{1h} - \frac{\Delta t}{2}A_{2h}\right)\mathbf{U_{CN}^{m+1}} = \left(I + \frac{\Delta t}{2}A_{1h} + \frac{\Delta t}{2}A_{2h}\right)\mathbf{U_{CN}^{m}} \tag{10}$$

for Δt the time step and $\mathbf{U_{CN}^{m}}$ represents the compact nodal approximation $[\bar{U}, V, W]^T$ at time $t = m\Delta t$. Discrete identity (10) can be replaced by the following factorization after neglecting the term $A_{1h}A_{2h}(\mathbf{U_{CN}^{m+1}} - \mathbf{U_{CN}^{m}})$ which is $O(\Delta t^2)$

$$\left(I - \frac{\Delta t}{2}A_{1h}\right)(I - \frac{\Delta t}{2}A_{2h})\mathbf{U_{CN}^{m+1}} = \left(I + \frac{\Delta t}{2}A_{1h}\right)(I + \frac{\Delta t}{2}A_{2h})\mathbf{U_{CN}^{m}} \tag{11}$$

The application of the Peaceman-Rachford (PR) decomposition to the above formulation lead to a calculation in two stages

$$\left(I - \frac{\Delta t}{2}A_{1h}\right)\mathbf{U_{CN}^{\frac{m+1}{2}}} = \left(I + \frac{\Delta t}{2}A_{2h}\right)\mathbf{U_{CN}^{m}} \tag{12}$$

$$\left(I - \frac{\Delta t}{2}A_{2h}\right)\mathbf{U_{CN}^{\frac{m+1}{2}}} = \left(I + \frac{\Delta t}{2}A_{1h}\right)\mathbf{U_{CN}^{m}}, \tag{13}$$

each of which alternates the application of operators A_{1h} and A_{2h} and so the direction of solving implicit one-dimensional linear systems (ADI methodology). The intermediate approximation $\mathbf{U_{CN}^{\frac{m+1}{2}}}$ is only used as an auxiliary term in above (14) formulation, but unnecessary in the final computational implementation as briefly explained below.

2.1.3. ADI implementation details

The calculation of $[\bar{U}, V, W]^{\frac{m+1}{2}}$ by the first stage of the PR-ADI algorithm involves two set of linear systems for the rows of $\bar{U}^{\frac{m+1}{2}}$ and $V^{\frac{m+1}{2}}$

$$\begin{cases} \bar{U}^{\frac{m+1}{2}}\bar{P}^T + \frac{\Delta t}{2}V^{\frac{m+1}{2}}\bar{Q}^T = \bar{U}^m\bar{P}^T - \frac{\Delta t}{2}\left(\bar{P}^{-1}\bar{Q}W^m\bar{P}^T\right) \\ V^{\frac{m+1}{2}}P^T + \frac{\Delta t}{2}U^{\frac{m+1}{2}}Q^T = V^mP^T \end{cases} \tag{14}$$

These vector equations can be decoupled by incorporating a fixed-point iteration that starts from $V_{(0)} = V^m$, and for $k = 0, 1, 2, \cdots$ solves the two following one-dimensional tridiagonal systems

$$\begin{cases} \bar{U}_{(k+1)}\bar{P}^T &= a_i - \frac{\Delta t}{2} V_{(k)}\bar{Q}^T \\ V_{(k+1)}P^T &= b_i - \frac{\Delta t}{2} U_{(k+1)}Q^T \end{cases} \tag{15}$$

where time related super indexes have been dropped to facilitate notation and new sub indexes indicate steps of inner fixed-point iteration. Vectors a_i and b_i denote known terms in (14) from the mth time level. Here, we adopt absolute differences $\left\|\bar{U}_{(k+1)} - \bar{U}_{(k)}\right\| <= tol$ and $\left\|V_{(k+1)} - V_{(k)}\right\| <= tol$ as the stop criteria for this inner iteration. The implementation of second stage of the (PR-ADI) decomposition is also implemented is a similar decoupled fashion to obtain $\bar{U}^{m+1}$ and W^{m+1}.

2.2. Mimetic compact scheme on staggered grids

2.2.1. Review of 1-D operators

Castillo and collaborators in [3] and [4] construct second-, fourth-, and sixth-order accurate numerical differentiation operators G and D on 1-D staggered grids, and they satisfy a discrete analog of the integration-by-part formula

$$\int_{0,1} (u'v + uv')dx = u(1)v(1) - u(0)v(0) \tag{16}$$

The preservation of this conservation property in the discrete justify their name as mimetic. Matrix structure of D and G is determined by the grid distribution of evaluations of smooth fields $u(x)$ and $v(x)$ on $[0, 1]$. In the case of v, Authors simply consider a nodal distribution of discrete v_i spaced by h and all collected in vector $V = [v_0, ..., v_N]^T$, i.e., this discrete field take the place of nodal U in above nodal CFD formulation. Instead, evaluations of $u(x)$ are staggerly located at cell centers $x_{i+\frac{1}{2}} = -1 + (i + \frac{1}{2})h$ for $i = 0, ..., N - 1$, and joint to boundary values u_0 and u_N, conform the approximate vector $U = [u_0 u_{\frac{1}{2}} ... u_{N-\frac{1}{2}} u_N]^T$. Mimetic approximations to $\frac{dv}{dx}$ are computed at cell centers by the product DV, while components of GU are the mimetic estimates of $\frac{du}{dx}$ calculated at all grid nodes including both boundaries. Second-order accurate G and D are given by

$$hD_2 = \begin{pmatrix} -1 & 1 & & & & & \\ & -1 & 1 & & & & \\ & & & \ddots & \ddots & & \\ & & & & -1 & 1 & \\ & & & & & -1 & 1 \end{pmatrix} \in R^{N\times(N+1)}, \quad hG_2 = \begin{pmatrix} -\frac{8}{3} & 3 & -\frac{1}{3} & & & \\ 0 & -1 & 1 & & & \\ & & \ddots & \ddots & & \\ & & & -1 & 1 & 0 \\ & & & \frac{1}{3} & -3 & \frac{8}{3} \end{pmatrix} \in R^{(N+1)\times(N+2)} \tag{17}$$

Matrix sub-indexes indicates the nominal accuracy of above mimetic operators and similar notation is adopted for their higher-order counterparts. Taylor expansions can be easily used to verify the second-order accuracy of above G_2 and D_2, and a similar, but more laborious task can be undertaken in the case of G_4 and D_4. Actually, the construction

procedure in [3] and [4] yields an individual three-parametric family for each one of these fourth-order operators, whose stencil bandwidth vary according to parameter choice finally selected (with a maximum bandwidth of 6 for lateral stencils at boundaries, and a minimum bandwidth of 4 for central stencils applied at interior points). We refer the interested reader to original references for a direct inspection, and we instead revise the compact factorization proposed by Abouali and Castillo in [1] of G_4 and D_4. Authors decompose the former operator G_4 as the product of an auxiliary operator R_G^4 by the second-order G_2, i.e., $G_4 = R_G^4 G_2$. The bandwidth of every stencil in R_G^4 is smaller by 1 respect to its counterpart in G_4, thus the nested application $R_G^4(G_2 U)$ represents an explicit compact differentiation of field $u(x)$. A similar auxiliary operator R_D^4 with a reduced bandwidth respect to D_4 is also given in [1], and allows approximating $\frac{dv}{dx}$ by the CFD formula $R_D^4(D_2 V)$. In this work, we incorporate the following choices for R_G^4 and R_D^4

$$\underbrace{\begin{pmatrix} \frac{503}{399} & -\frac{1234}{2003} & \frac{551}{1217} & \frac{-719}{7198} & \frac{25}{9768} & 0\cdots \\ -\frac{2}{35} & \frac{941}{840} & -\frac{29}{420} & \frac{1}{168} & 0 & 0\cdots \\ 0 & -\frac{1}{24} & \frac{13}{12} & -\frac{1}{24} & 0 & 0\cdots \end{pmatrix}}_{R_G^4}, \quad \underbrace{\begin{pmatrix} \frac{1045}{1142} & \frac{492}{2291} & -\frac{418}{2371} & \frac{328}{6821} & -\frac{25}{15576} & 0\cdots \\ -\frac{1}{24} & \frac{13}{12} & -\frac{1}{24} & 0\cdots & & \\ 0 & -\frac{1}{24} & \frac{13}{12} & -\frac{1}{24} & 0\cdots & \end{pmatrix}}_{R_D^4}$$

2.2.2. Extension to 2-D with Crank-Nicolson time integration

Mimetic CFD discretization of continuous acoustic fields in (1) takes place on the staggered grid shown in figure 1. Again, we consider an uniform grid step h in both directions and a total of $N \times N$ square cells, just for the clarity of formulation below (see, left panel in figure 1). Discrete values of u are located at cell centers, at the central point of boundary edges, and also at the four grid corners. In this way, the gradient component $\frac{\partial u}{\partial x}$ can be approximated by the application of operator $R_G^4(G_2)$ along of these u grid-lines in the x direction. These approximations share same grid sites with velocity v (see, right panel in figure 1). In a similar manner, grid locations of velocity w also hold mimetic approximations to $\frac{\partial u}{\partial y}$ computed by the application of same operator along u grid-lines in the y direction. Notice that the grid distribution of velocity components v and w is a consequence of their spatial dependency on ∇u according to the wave equation (1). At the implementation level, matrices U, V, and W collecting mimetic values of pressure and velocities have different dimensions of $(N+2) \times (N+2)$, $(N+2) \times (N+1)$, and $(N+1) \times (N+2)$, respectively. In this method, we also require of reduced matrix $\bar{V}$ obtained from V after removing first and last rows, as well as of reduced matrix $\bar{W}$ derived from W by omitting first and last columns. Mimetic CFD approximation to $\nabla \cdot \vec{v}$ is exclusively computed at cell centers and given by the matrix $\bar{V}(R_D^4 D_2)^T + (R_D^4 D_2)\bar{W}$ over the whole grid, where composed operator $R_D^4 D_2$ must has appropriate dimensions.

The following mimetic CFD formulation proceeds analogously to the former case of nodal CFD discretization, and we next remark only main differences. First, spatial differentiation operators in (9) are now replaced by

$$A_{1h}\begin{bmatrix} \bar{U} \\ V \\ W \end{bmatrix} = -\begin{bmatrix} \bar{V}(R_D D_2)^T \\ U(R_G G_2)^T \\ 0 \end{bmatrix}, \quad A_{2h}\begin{bmatrix} \bar{U} \\ V \\ W \end{bmatrix} = -\begin{bmatrix} R_D D_2 \bar{W} \\ 0 \\ R_G G_2 U \end{bmatrix}$$

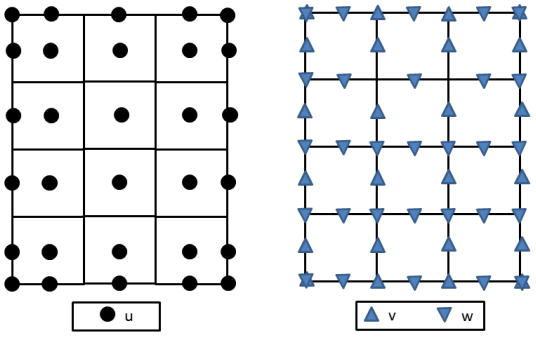

Figure 1: Mimetic FD discretization of continuous acoustic fields in (1) on a 2-D staggered grid

Above operators fit nicely into the Crank-Nicolson time integration of the acoustic model (1) followed by the PR decomposition, and given by equations (10-13). Now, individual equations for intermediate approximation matrices U^*, V^*, and W^*, become

$$\begin{cases} \bar{U}^* + \frac{\Delta t}{2}(\bar{V}^* D_2^T) R_D^T = \bar{U}^m - \frac{\Delta t}{2} R_D (D_2 \bar{W}^m) \\ \bar{V}^* + \frac{\Delta t}{2}(\bar{U}^* G_2^T) R_G^T = V^m \\ \bar{W}^* = W^m - \frac{\Delta t}{2} R_G (G_2 U^m) \end{cases} \tag{18}$$

Again, matrix W^* is readily determined by last equation, and U^* and V^* are coupled in the subsystem defined by the first two equations. In order to use one-dimensional compact differentiation, this subsystem is solved by a similar fixed-point iteration to (15) with appropriate independent matrix terms a_i and b_i. The second stage of this PR decomposition yield V^{m+1} by an explicit calculation, and U^{m+1} and W^{m+1} after convergence of the corresponding inner fixed-point iteration.

3. Mimetic leap-frog scheme on staggered grids

As mentioned in the introduction section, modern FD methods for acoustic wave propagation are designed on spatial staggered grids and use explicit time integration strategies. Thus, we combine the fourth order mimetic discretization based on operators G_4 and D_4 to a second order Leap-Frog time integration to implement a conventional method for the acoustic model (1). This method results staggered in both, space and time, and represents a simplified version of the mimetic scheme used by Rojas and co-workers in [25] for elastic wave propagation.

$$\begin{cases} \bar{U}^{m+1} = \bar{U}^m - \Delta t (\bar{V}^{m+\frac{1}{2}} D_2^T + D_2 \bar{W}^{m+\frac{1}{2}}) \\ V^{m+\frac{1}{2}} = V^{m-\frac{1}{2}} - \Delta t (U^m G_4^T) \\ W^{m+\frac{1}{2}} = W^{m-\frac{1}{2}} - \Delta t (G_4^T U^m) \end{cases} \tag{19}$$

Above, super indexes on approximation matrices remark the time staggering evolution of this scheme. In next section, results from this Leap-Frog mimetic scheme are used as reference basis for comparing experimental convergence and computer time consumption of both CFD methods.

4. Results and discussion

The acoustic model (1) accepts the following harmonic analytical solution

$$u = \text{sen}(\frac{2\pi x}{\lambda})\,\text{sen}(\frac{2\pi y}{\lambda})\cos(\frac{2\pi t}{T}) \tag{20}$$

in case that wave speed $c = \sqrt{\frac{k}{\rho}}$ satisfies the dispersion relation $c = \frac{\lambda}{T}$, where λ and T stand for the spatial and time periods of the exact solution, respectively. Note that Dirichlet boundary conditions defined in (1) are reduced to the homogeneous case. We next derive a family of numerical tests where the total number of grid cells N defines the grid resolution as the number of nodes sampling the only travelling wavelength, $N\lambda$. Computational meshes with $N\lambda \leq 4$ are poorly-resolved grids given that the grid sampling is close to the theoretical Nyquist limit ($N\lambda = 2$). Such simulation for a FD fourth-order scheme can be referred as a hard test. On the other hand, we might call as well-resolved those grids where $6 \leq N\lambda \leq 8$, and highly-resolved grids those that support a wavelength sampling of $N\lambda \geq 10$. Naturally, simulation accuracy must increase as test switches from hard, to mild (on well-resolved grids), and finally to an easy test (on highly-resolved grids). Here, we select $\lambda = \frac{1}{4}$ and perform nine simulations with each of the numerical schemes formulated in previous section using a common range of grid cells $N = 8, 16, 32, 48, 64, 96, 128, 192, 256$. In this way, grid resolution improves progressively, $N\lambda = 2, 4, 8, 12, 16, ...$ Time step Δt is taken according to a Courant-Friedrichs-Lewy stability bound cfl^{max}, where $\Delta t = c^{-1}hcfl^{max}$. This limit cfl^{max} depends on each particular method and exhaustive numerical experimentation leads to values reported in Table 1. In this exploratory analysis, we use as reference for the Leap-frog mimetic scheme the known Von-Neumann condition for modeling acoustic and elastic wave propagation in unbounded and homogeneous domains under staggered discretization: $h^{-1}c\Delta t \leqslant (\sqrt{2}\Sigma_{k=1}^{n}|C_k|)^{-1}$ (see for instance, [8] [28]). Here, C_k are the stencil coefficients for central differentiation in space with accuracy $O(h^{2n})$. In our case, these coefficients correspond to the staggered inner stencil of matrices G_4 and D_4.

Table 1: Courant-Friedrichs-Lewy stability limits, range of total iterations, and estimated convergence rates observed on numerical simulations

Scheme	cfl^{MAX}	Number of iterations (minimum;maximum)	Convergence rates (Tsim= $5T$)	Convergence rates (Tsim= $20T$)
Compact nodal	0.91	(31;3957)	4.04	3.80
Compact mimetic	0.81	(35;4442)	4.71	4.40
Leap-frog mimetic	0.45	(63;8045)	1.97	1.95

Figures 2a and 2b depict absolute errors in Frobenius norm of computed numerical solutions by each scheme when the simulation time varies from Tsim= $5T$ to Tsim= $20T$, respectively. These experiments allow assessing the

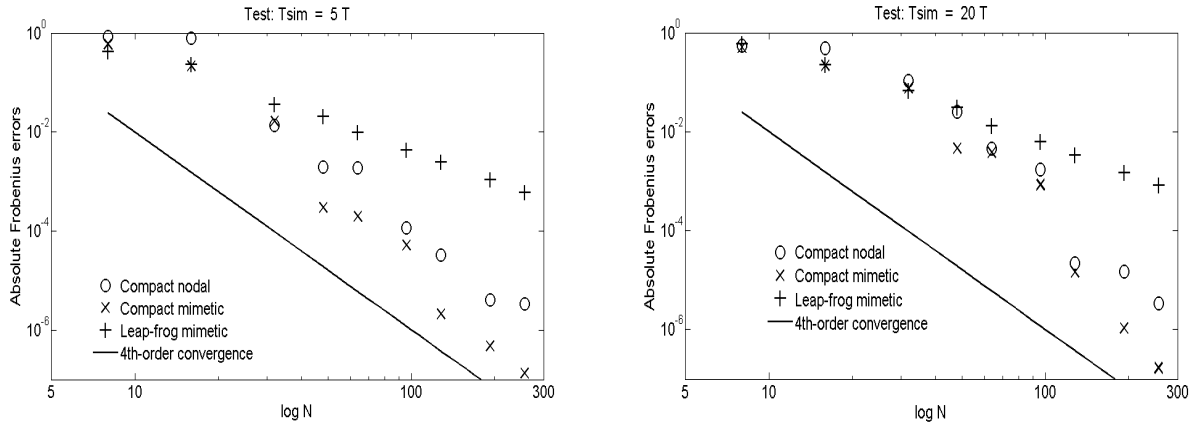

(a) (b)

Figure 2: Comparison of absolute errors in Frobenius norm of computed numerical solutions by each scheme when the simulation time is: (a) Tsim= $5T$; (b) Tsim= $20T$

behaviour of solution accuracy and heuristic convergence when numerical schemes perform a short-term simulation (total iterations $\sim$ 10) and later a long-term simulation (total iterations $\sim$ 1000). A qualitative comparison of these figures indicates that both CFD schemes yield misfits more scattered and much smaller on highly-resolved grids ($N \geq 48$) than those delivered by the mimetic Leap-frog scheme. Only on grids with poor or mild resolution ($N \leq 48$), accuracy achieved by these three schemes is comparable, with certain gain shown by both mimetic methods. For instance, errors rendered by these methods are only 30% of those observed on nodal CFD solutions when $N = 16$. This accuracy advantage is a consequence of the staggered differentiation that halves the grid spacing compared to a nodal FD formula. Only the mimetic CFD scheme mantains this accuracy superiority on highly-resolved grids due to its faster convergence. In our finest gridding simulations ($N = 256$), this scheme delivers errors that are only 5% and 2% of those misfits observed on similar nodal CFD solutions to both tests. We use linear least-square fitting to error data depicted in these log-scale figures, to estimate experimental convergence rates for each scheme as N increases, and results are also given in Table 1. Both compact schemes show an approximately fourth-order convergence compared to the Leap-Frog staggered scheme that only displays a second-order accuracy. This is a strong indication that time discretization errors arising from the Crank-Nicolson time integration preserve the spatial accuracy of fourth-order FD, which is not achieved by the Leap-frog technique.

Figure 3 shows the computation times of nodal CFD simulations in both tests relative to corresponding measures recorded on mimetic CFD simulations. Omitting the anomalous record for the coarsest grid ($N = 8$), we observe that the former scheme spends between four and five times the execution times measured during mimetic CFD simulations. Even though, the nodal CFD scheme presents larger cfl^{max} limit, and therefore requires of fewer iterations to achieve same simulation time Tsim, the solution of its embedded tridiagonal linear systems lead to a higher computational cost compared to the explicit differentiation applied by the CFD mimetic method. Notice that this is the main difference

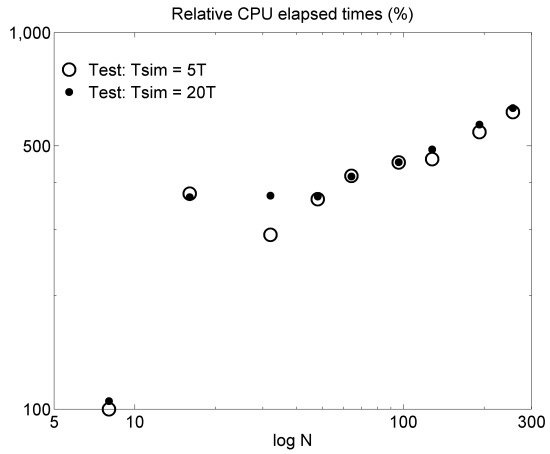

Figure 3: Computation times of nodal CFD simulations relative to corresponding mimetic CFD execution times when Tsim varies from $5T$ to $20T$

on the formulation and computational implementation of both CFD schemes.

5. Conclusions

In this work, we employ fourth-order mimetic CFD to discretize the velocity-pressure formulation of the acoustic wave equation on 2-D staggered meshes. In time, we apply the Crank-Nicolson formulation in combination to the Peaceman-Rachford splitting technique to allow updating discrete fields by alternating the coordinate direction of CFD differentiation (ADI-like iterations). Mimetic CFD offers an explicit differentiation, therefore this new scheme is free of solving any embedded linear systems as it is indeed required by classical implicit CFD. As a comparing reference, we also use fourth-order implicit CFD to implement an alternative solver on nodal grids. In our numerical experimentation, we only consider uniform grids with step h and solve a test with a harmonic exact solution with spatial period λ that satisfy homogeneous Dirichlet boundary conditions. Simulations provide evidence that this nodal CFD scheme presents a larger Courant-Friedrichs-Lewy stability limit $cfl^{Max} \sim 0.91$ compared to the one induced from mimetic CFD results $cfl^{Max} \sim 0.81$. However, latter simulations only spend between a $\frac{1}{4}$ or even a $\frac{1}{5}$ of the execution time of the former experiments on a broad set of grids with resolution varying in $4 \leq N\lambda \leq 64$. This computational advantage of the mimetic CFD scheme is accompanied with higher accuracy on highly-resolved grids $N\lambda \geq 12$. Least square fitting of error data reveal that convergence rates of both CFD schemes are approximately 4, but those shown by the mimetic scheme are slightly bigger. We additionally implement a staggered fourth-order FD scheme using standard (non compact) mimetic operators in space and coupled to second-order Leap-frog time integration. This method exhibits most important features of modern explicit FD schemes used for wave propagation. In same numerical tests, this scheme shows a nearly quadratic convergence and equates accuracy of CFD methods only in simulations with grid resolution varying $N\lambda \leq 12$. This last observation opens ground for the mimetic CFD modeling of acoustic motion on more general applications in areas like geophysics or electro-magnetics.

References

[1] Abouali M. and Castillo J. E. High-order compact Castillo-Grone's Mimetic Operators. Report of Computational Science Research Center at San Diego State University. CSRCR02 1-13, 2012.

[2] Brio M., Zakharian A., Webb G. Numerical time-dependent partial differential equations for scientist and engineers. Mathematics in Science and Engineering. Academic Press, first edition, Vol. 213, 1-312, 2010.

[3] Castillo J., Hyman J. M., Shashkov M. and Steinberg, S. Fourth- and sixth-order conservative finite difference approximations of the divergence and gradient. Applied Numerical Mathematics: Transactions of IMACS 37 (1-2), 171-187, 2001.

[4] Castillo, J., and Grone, R. A matrix analysis approach to higher-order approximations for divergence and gradients satisfying a global conservation law. SIAM J. Matrix Anal. Appl. 25, 128-142, 2003.

[5] Castillo, J. and Yasuda M. Linear systems arising for second-order mimetic divergence and gradient discretizations. J. Math. Model. Algorithm 4 (1), 67-82, 2005.

[6] Carcione J. M., Finetti I. R. and Gei D. Seismic modeling study of the earth's deep crust. Geophys. 68 (2), 656-664, 2003.

[7] Carpenter M., Gottlieb D., Abarbanel S. Stable and accurate boundary treatments for compact, high-order finite-difference scheme. Appl. Numer. Math. 12, 55-87, 1993.

[8] Dablain M. A. The application of high-order differencing to the scalar wave equation. Geophys. 51, 54-66, 1986.

[9] Dai W. and Nassar R. Compact ADI method for solving parabolic differential equations, Numer. Meth. Part. Differ. Equat. 18 (2), 129-142, 2002.

[10] Douglas J. and Peaceman D. W. Numerical solution for two-dimensional heat flow problems, Am. Inst. Chem. Eng. J. 1 (4), 505-512, 1955.

[11] Ekaterinaris J. A. Implicit, high-resolution compact schemes for gas dynamics and aeroacoustics. J. Comput. Phys. 156, 272-299, 1999.

[12] Etgen J. T., O'Brien M. J. Computational methods for large-scale 3D acoustic finite-difference modeling tutorial. Geophys. 72 (5), SM223-SM230, 2007.

[13] Graves, R., Simulating seismic wave propagation in 3D elastic media using staggered-grid finite differences. Bull. Seis. Soc. Am. 86, 1091-1106, 1996.

[14] Gelis C., Leparoux D., Virieux J., Bitri A., Operto S. and G. Grandjean. Numerical modeling of surface waves over shallow cavities. J. of Environ. and Engin. Geophys., 10 (2), 111-121, 2005.

[15] Hestholm S. Elastic wave modeling with free surfaces: Stability of long simulations. Geophys. 68, 314-321, 2003.

[16] Jichun L., Yitung C. and Guoqing L. High-order compact ADI methods for parabolic equations. Comput. Math. Appl. 52 (8-9), 1343-1356, 2006.

[17] Kim S. and Lim H. High-order schemes for acoustic waveform simulation. Appl. Numer. Math., 57, 402-414, 2007.

[18] Lai M.-C. A simple compact fourth-order Poisson solver on polar geometry. J. Comput. Phys. 182 (1), 337-345, 2002.

[19] Lee C. and Seo Y. A new compact spectral scheme for turbulence simulations. J. Comput. Phys. 183, 438-469, 2002.

[20] Lele S. Compact finite difference schemes with spectral-like resolution. J. Comput. Phys. 103, 16-42, 1992.

[21] Liu Y., Wei X. C. Finite-difference numerical modeling with even-order accuracy in two-phase anisotropic media. App. Geophys. 5, 107-114, 2008.

[22] Peaceman D. W. and Rachford H. The numerical solution of parabolic and elliptic differential equations. J. Society for Indust. and Appl. Math. 3 (1), 28-41, 1955.

[23] Pitarka A. 3-D elastic finite-difference modeling of seismic motion using staggered grids with nonuniform spacing. Bull. Seism. Soc. Am. 89, 54-68, 1999.

[24] Qin J. The new alternating direction implicit difference methods for the wave equations. J. Comput. Appl. Math. 230, 213-223, 2009.

[25] Rojas O., Day S. M., Castillo J. and Dalguer L. Modeling of rupture propagation using high-order mimetic finite-differences. Geophys. J. Int. 172, 631-650, 2008.

[26] Rojas, O., Otero, B., Castillo, J. E. and Day, S. M. Low dispersive modeling of Rayleigh waves on partly staggered grids. Computational Geosciences, 1-17, 2013.

[27] Samarskii A. A., Tishkin V. F., Favorskii A. P. and Shashkov M. Y. Operational finite-difference schemes. Differential Equations 17(7), 854-862, 1981.

[28] Saenger, E.H., Gold, N., Shapiro, S.A. Modeling the propagation of elasticwaves using a modified finite-difference grid. Wave Motion 31, 77-92, 2000.

[29] Sakamoto S., Seimiya T. and Tachibana H. Visualization of sound reflection and diffraction using finite difference time domain method. Acoustical Science and Technology 23 (1), 2002.

[30] Strikwerda J. C. Finite difference schemes and partial differential equations. University of Wisconsin-Madison, SIAM, 2nd Edition, Madison, Wisconsin, 2004.

[31] Takenaka H., Nakamura T., Okamoto T. and Kaneda Y. A unified approach implementing land and ocean-bottom topographies in the staggered-grid finite-difference method for seismic wave modeling. Proceedings of the 9th SEGJ International Symposium, Japan, 1-4, 2009.

[32] Tolstykh M. A. Vorticity-divergence semi-lagrangian shallow-water model of the sphere based on compact finite differences. J. Comput. Phys. 179 (1), 180-200, 2002.

[33] Virieux, J. P-SV wave propagation in heterogeneous media: Velocity-stress finite-difference method. Geophys. 51, 889-901, 1986.

[34] Visbal M. R. and Gaitonde D. V. On the use of higher-order finite-difference schemes on curvilinear and deforming meshes. J. Comput. Phys. 181 (1), 155-185, 2002.

[35] Vossen V. R., Robertsson J. O. A. and Chapman C. Finite-difference modeling of wave propagation in a fluid-solid configuration. Geophysics, 67, 618-624, 2002.